Supplementary Information (SI) for Materials Horizons.
This journal is © The Royal Society of Chemistry 2025

Supporting Information

Acetylene Semi-Hydrogenation Catalyzed by Pd Single Atom Sandwiched in Zeolitic Imidazolate Frameworks via Hydrogen Activation and Spillover

Yan-Ting Li[a#], Wen-Gang Cui[a,b#], Ying-Fei Huo[a], Lei Zhou[a], Xinqiang Wang[b], Fan Gao[b], Qiang Zhang[a], Wei Li[a], Tong-Liang Hu[a,*]

a. School of Materials Science and Engineering, National Institute for Advanced Materials, Nankai University, Tianjin, 300350, China E-mail: tlhu@nankai.edu.cn (T.-L. Hu)

b. Institute of Science and Technology for New Energy, Xi'an Technological University, Xi'an 710021, China

# Y.-T. Li and W.-G. Cui contributed equally to this work.

Catalyst characterization

The morphologies of the samples were observed using the field emission scanning electron microscopy SEM-EDS system (Zeiss Gemini Ultra). Transmission electron microscopy (TEM) images of the samples were obtained by HRTEM-EDX (Philips TecnaiG2 F20 microscope). The aberration-corrected high-angle annular dark-field scanning transmission electron microscopy (AC HAADF-STEM) images were obtained by a field-emission transmission electron microscope (JEOL JEM-ARM 200F) equipped with a dual spherical aberration corrector. Thermogravimetric analysis (TGA) was recorded under an air atmosphere from room temperature to 800 °C using a Rigaku standard thermogravimetry-differential thermal analysis (TG-DTA) analyzer at a heating rate of 10 °C min^{-1}. Powder X-ray diffraction (PXRD) patterns were collected on a Rigaku MiniFlex 600 diffractometer at 20 kV and 15 mA with Cu Kα radiation (λ = 1.5418 Å) using a scan rate of 10.0 ° min^{-1} in the 2θ range from 3 to 50 ° under an air atmosphere. The Pd contents were analyzed by inductively coupled plasma optical emission spectrometry (ICP-OES) analysis on Perkin-Elmer 3300DV instrument. X-ray photoelectron spectroscopy (XPS) was performed on ESCALAB 250Xi X-ray photoelectron spectrometer with Al Kα (1486.6 eV) radiation source. Fourier transform infrared spectra (FT-IR) were recorded on a Bruker TENSOR 37. In situ Fourier transform infrared spectra were collected using an FTIR spectrometer (BRUKER Tensor II), equipped with a liquid N_2 cooled mercury−cadmium−telluride detector. C_2H_2-temperature-programmed desorption (C_2H_2-TPD) was performed by using a chemisorption analyzer (Autochem 2950HP) from Micromeritics. The Pd K-edge XAFS analyses were performed with Si(111) crystal monochromators at the BL14W Beam line at the Shanghai Synchrotron Radiation Facility (SSRF) (Shanghai, China). Hydrogen spillover detection by WO_3 was performed according to the following procedures. The mixture of 1 g of WO_3 and 0.02 g of catalyst was placed in a quartz tube and held in place with silica wool. After exposure of the powder to hydrogen (100 mL·min^{-1}) at 30 °C for 10 min, the hydrogen flow was switched off, and the quartz tube was removed from the oven to observe the color changes of the powder

samples.

Computational Methods

All density functional theory (DFT) calculations were performed using the Vienna Ab initio Simulation Package (VASP)[1,2] at the level of generalized gradient approximation (GGA) using Perdew-Burke-Ernzerhof (PBE) exchange-correlation functional.[3] Projector-augmented wave (PAW) potentials were used to describe the effective cores.[4,5] The valence electrons of all atoms were expanded in a plane wave basis set with a cutoff energy of 400 eV. The atomic structures were relaxed using either the conjugate gradient algorithm or the quasi-Newton scheme until the forces were less than 0.05 eV/Å for all unconstrained atoms, and the energy convergence criteria for all self-consistent field calculations were set as 10^{-5} eV. The DFT-D3 method developed by Grimme was employed to treat the van der Waals interactions.[6] The lattice parameters of optimized Pd-ZIF-8 were $a = b = c = 16.991$ Å. Brillouin zone was sampled with Γ point due to the large size of the unit cell.[7]

The adsorption energy was defined as

$$E_{ads} = E(\text{ZIF-8/M}) - E(\text{ZIF-8}) - E(\text{M}) \quad (1)$$

where the E(ZIF-8 /M), E(ZIF-8) and E(M) represent the total energies of MOF with the adsorbate, the optimized ZIF-8 structure and the isolated molecule, respectively. A positive value corresponds to an endothermic process, whereas a negative value indicates the process is exothermic.

Figures and Tables

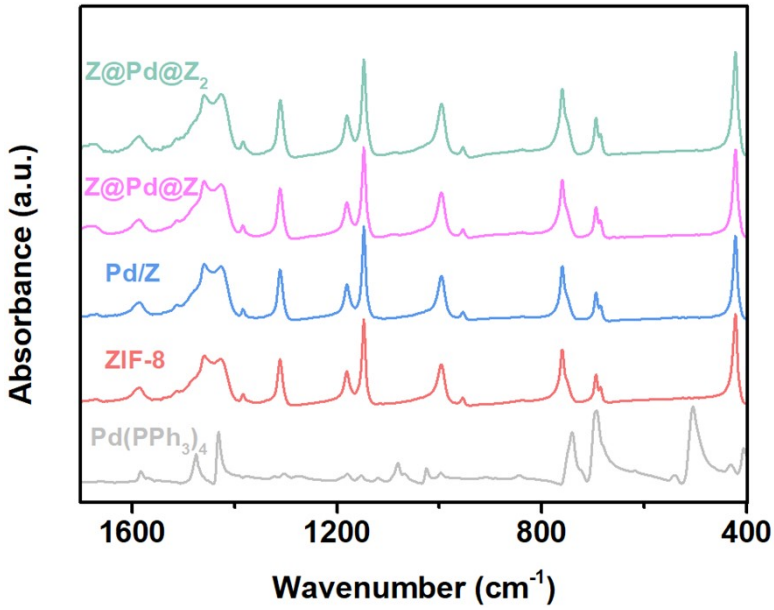

Fig. S1. FTIR spectra of $Pd(PPh_3)_4$, ZIF-8, Pd/Z and $Z@Pd@Z_x$.

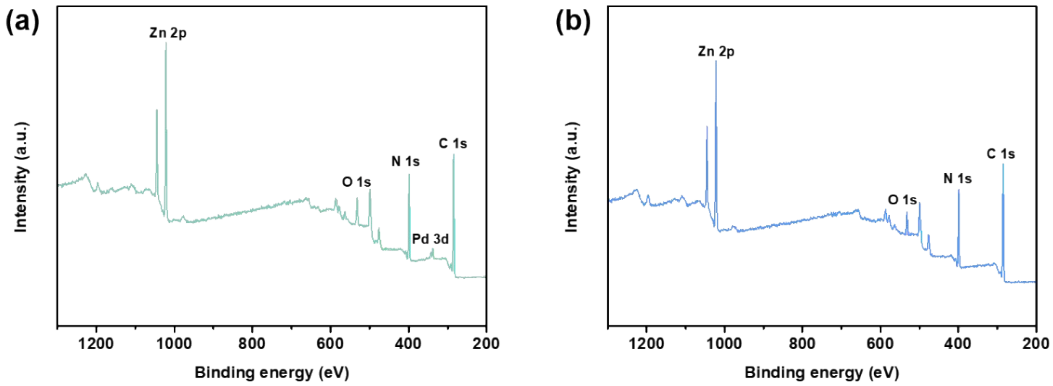

Fig. S2. XPS survey spectra of (a) Pd/Z and (b) Z@Pd@Z.

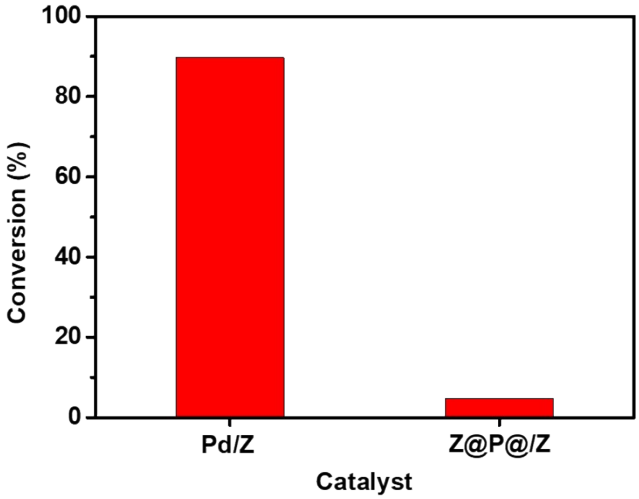

Fig. S3. Phenylacetylene hydrogenation conversion on Pd/Z and Z@Pd@Z. Reaction condition: 0.5 mmol phenylacetylene, 10 mL isopropanol, 50 mg catalyst, 80 °C, 2 MPa, 2 h.

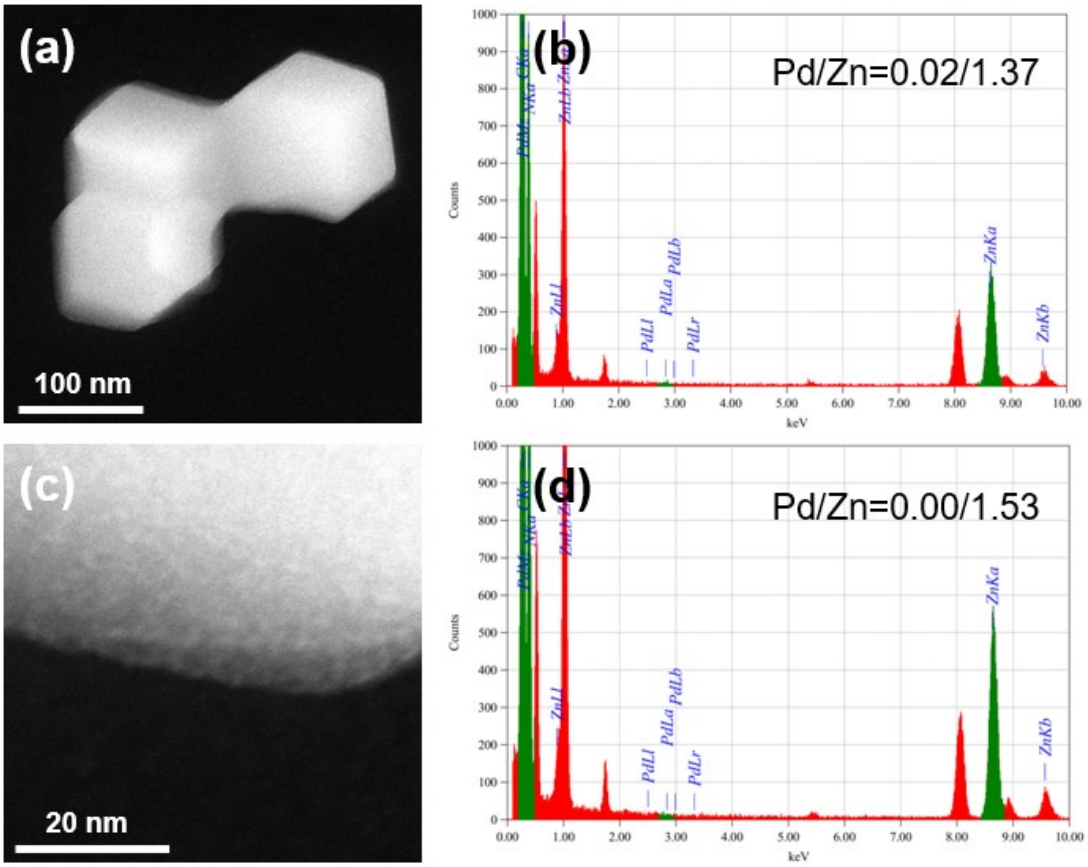

Fig. S4. TEM images and quantitative analysis of the bulk (a) and the edge (b) of Z@Pd@Z catalyst, Pd/Zn was the atomic ratio.

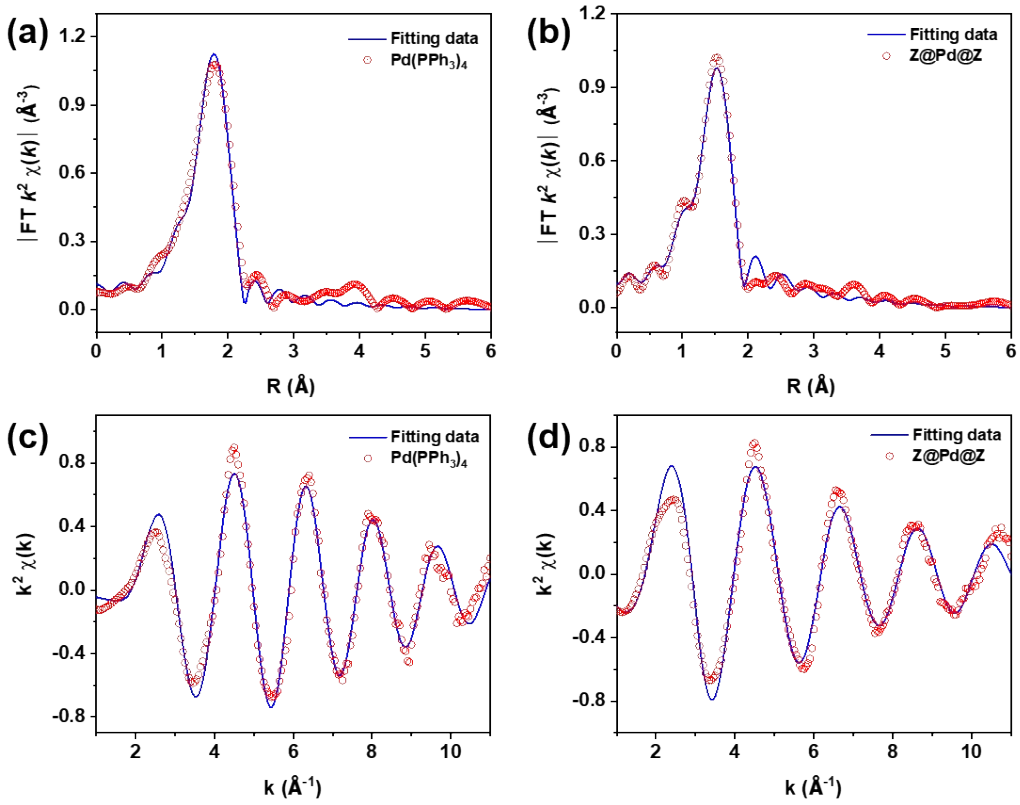

Fig. S5. Pd K-edge EXAFS (points) and fit (line) shown in k^2 weighted *R*-space of (a) $Pd(PPh_3)_4$ and (b) Z@Pd@Z; Pd K-edge EXAFS (points) and fit (line) shown in k^2 weighted *k*-space of (c) $Pd(PPh_3)_4$ and (d) Z@Pd@Z.

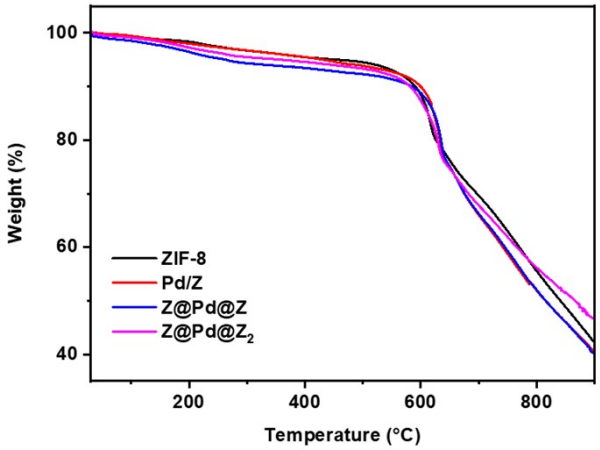

Fig. S6. The TG curves of ZIF-8, Pd/Z, Z@Pd@Z and $Z@Pd@Z_2$.

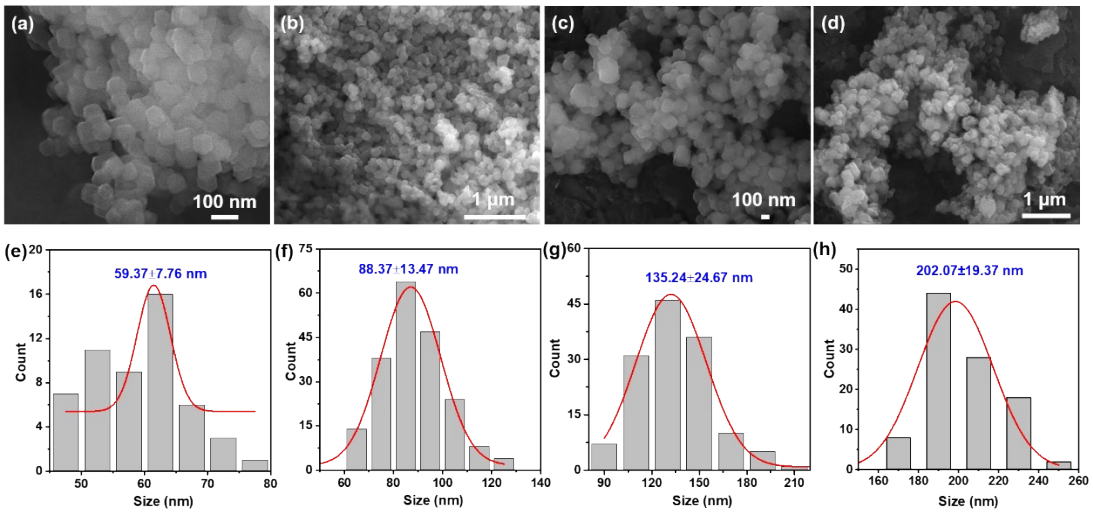

Fig. S7. SEM images and corresponding particle size distribution of (a, e) Pd/Z, (b, f) Z@Pd@Z, (c, g) Z@Pd@Z_2 and (d, h) Z@Pd@Z_3.

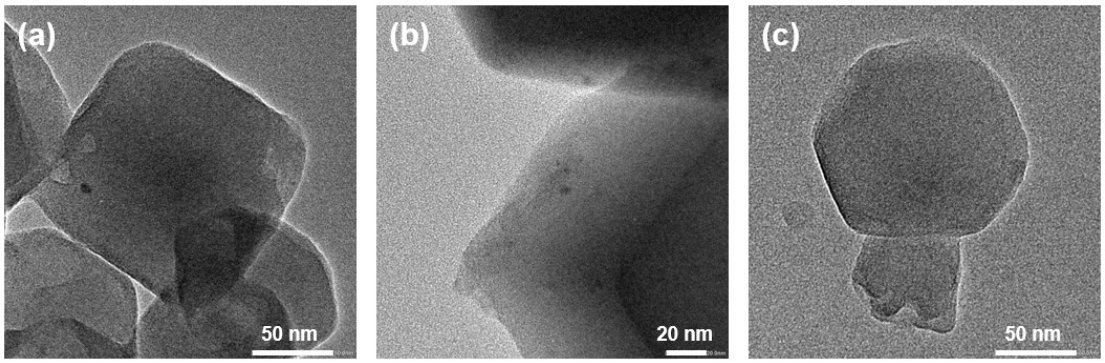

Fig. S8. TEM images of (a) Pd_{NPs}/Z and (b) Pd/Z, (c) Z@Pd@Z after 120 °C reaction.

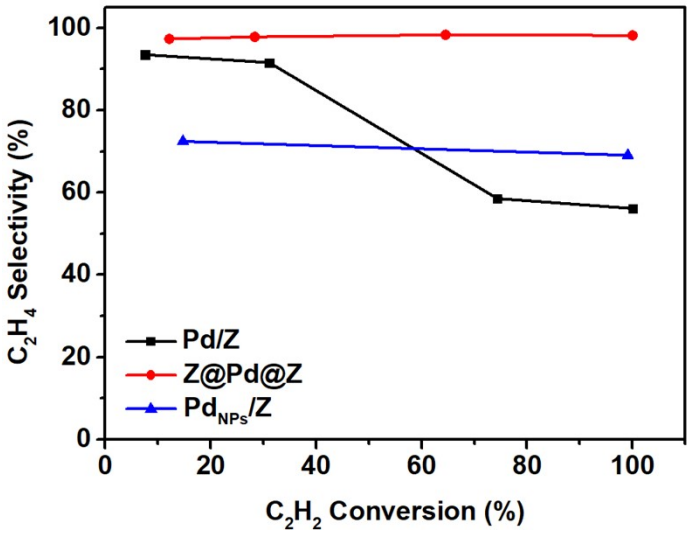

Fig. S9. Selectivity to C_2H_4 versus conversion of C_2H_2 over Pd/Z, Z@Pd@Z and P_{NPs}/Z catalysts.

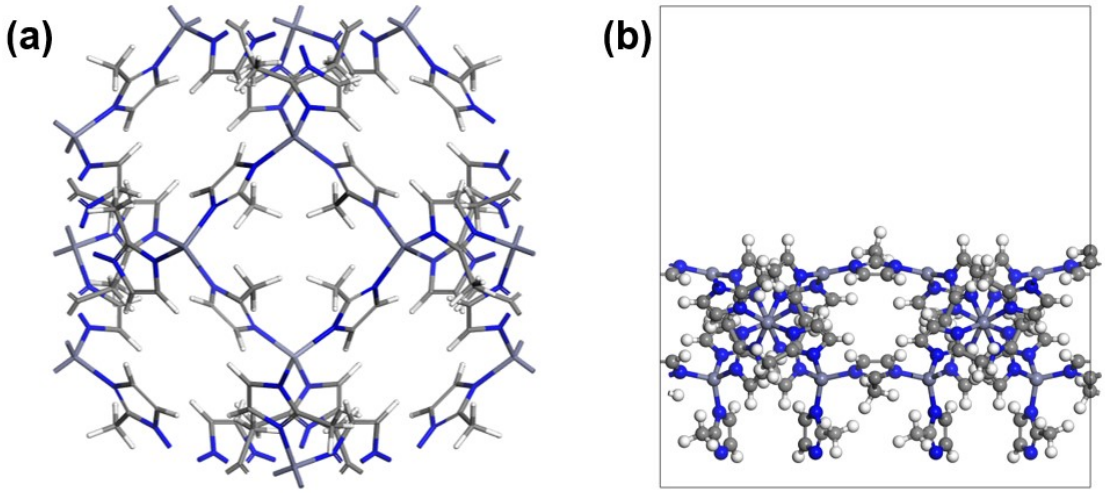

Fig. S10. Structure of (a) ZIF-8 and (b) ZIF-8 (110) surface.

Table 1. Fitting parameters for Pd K-edge EXAFS for the samples.

Sample	Shell	CN[a]	R(Å)[b]	σ^2(Å^2)[c]	ΔE_0(eV)[d]	S_0^2	R factor
Pd foil	Pd-Pd	12(set)	2.74	0.006	3.3±0.2	0.8565	0.003
$Pd(PPh_3)_4$	Pd-P	4.1±0.2	2.33	0.006	-3.1±0.5	0.8565(set)	0.016
Z@Pd@Z	Pd-N	3.8±0.2	2.04	0.003	3.4±0.5	0.8565(set)	0.015

[a]*CN*, coordination number; [b]*R*, the distance to the neighboring atom; [c]σ^2, the Mean Square Relative Displacement (MSRD); [d]ΔE_0, inner potential correction; *R* factor indicates the goodness of the fit. S_0^2 was fixed to 0.8565, according to the experimental EXAFS fit of the sample foil by fixing *CN* as the known crystallographic value. This value was fixed during EXAFS fitting, based on the known structure of Pd foil. Data range $3.0 \leq k \leq 11.0$ Å^{-1}, $1.0 \leq R \leq 2.5$ Å. The Debye-Waller factors and ΔRs are based on the *guessing* parameters and constrained for Pd-P and Pd-N.

Table S2. Pd content and particle size on ZIF derived catalysts.

Catalyst	Pd wt%[a]	Pd atom%[b]	Pd wt%[c]	Average Size nm[d]	Outer layer thickness nm[d]
Pd/Z	0.047	0.43	0.04	59.37	-
Z@Pd@Z	0.008	0.00	0.01	88.37	14.50
$Z@Pd@Z_2$	0.005	-	-	135.24	37.94
$Z@Pd@Z_3$	0.002	-	-	202.07	71.35

a. Pd content determined by ICP;

b. Pd content determined by XPS;

c. Pd content determined by EDS-mapping;

d. Particle size determined by size distribution.

Table S3. Recently reported high performance catalysts for selective hydrogenation of acetylene to ethene.

Catalysts	Temperature (°C)	Conversion (%)	Selectivity (%)	STY ($mL_{C2H4}·mg_{Pd}^{-1}·h^{-1}$)	Ref.
Z@Pd@Z	120	100	98.18	1872.69	This work
$Cu_{15}Pd@C$	120	100	91	-	8
PdAg/ r-TiO_2 benchmark	98	100	97.2	46.66	9
Pd_1Ag/SiO_2 SAA catalyst	173	100	92	56.33	10
Ag@Pd/SiO_2	108	100	95	58.16	10
Pd_1/ND@G	180	100	>90	490.91	11
Pd@SOD	150	99.8	94.5	171.47	12
Pd/CeO_2-600H	160	100	85	156.12	13
$Pd_{1.0}/Bi_2O_3/TiO_2$	44	90	91	42.73	14
Pd-$SrTiO_3$	100	98	92	1168.62	15

References

1 G. K. J. Furthmüller, *Phys. Rev. B*, 1996, **54**, 11169.

2 J. F. l. G. Kresse, *Comp. Mater. Sci.*, 1996, **6**, 15-50.

3 J. P. Perdew, K. Burke and M. Ernzerhof, *Phys. Rev. Lett.*, 1996, **77**, 3865.

4 P. E. Blochl, *Phys. Rev. B Condens. Matter Mater. Phys.*, 1994, **50**, 17953-17979.

5 D. J. G. Kresse, *Phys. Rev. B*, 1999, **59**, 1758.

6 S. Grimme, J. Antony, S. Ehrlich and H. Krieg, *J. Chem. Phys.*, 2010, **132**, 154104.

7 H. J. Monkhorst and J. D. Pack, *Phys. Rev. B*, 1976, **13**, 5188-5192.

8 C. Lu, S. Zhou, W. Zhou, C. Zhou, Q. Li, A. Zeng, A. Wang, L. Tan and L. Dong, *Chem. Eng. J.*, 2023, **464**, 142609.

9 L. Chen, X.-T. Li, S. Ma, Y.-F. Hu, C. Shang and Z.-P. Liu, *ACS Catal.*, 2022, **12**, 14872-14881.

10 F. Liu, Y. Xia, W. Xu, L. Cao, Q. Guan, Q. Gu, B. Yang and J. Lu, *Angew. Chem. Int. Ed.*, 2021, **60**, 19324-19330.

11 F. Huang, Y. Deng, Y. Chen, X. Cai, M. Peng, Z. Jia, P. Ren, D. Xiao, X. Wen, N. Wang, H. Liu and D. Ma, *J. Am. Chem. Soc.*, 2018, **140**, 13142-13146.

12 S. Wang, Z. J. Zhao, X. Chang, J. Zhao, H. Tian, C. Yang, M. Li, Q. Fu, R. Mu and J. Gong, *Angew. Chem. Int. Ed.*, 2019, **58**, 7668-7672.

13 Y. Guo, Y. Li, X. Du, L. Li, Q. Jiang and B. Qiao, *Nano Res.*, 2022, **15**, 10037-10043.

14 S. Zou, B. Lou, K. Yang, W. Yuan, C. Zhu, Y. Zhu, Y. Du, L. Lu, J. Liu, W. Huang, B. Yang, Z. Gong, Y. Cui, Y. Wang, L. Ma, J. Ma, Z. Jiang, L. Xiao and J. Fan, *Nat. Commun.*, 2021, **12**, 5770.

15 Z. Li, J. Zhang, J. Tian, K. Feng, Y. Chen, X. Li, Z. Zhang, S. Qian, B. Yang, D. Su, K. H. Luo and B. Yan, *ACS Catal.*, 2024, **14**, 1514-1524.